Journal of Advanced Research in Fluid Mechanics and Thermal Sciences

Journal homepage:
https://semarakilmu.com.my/journals/index.php/fluid_mechanics_thermal_sciences/index
ISSN: 2289-7879

Joint Effects of Brownian Motion and Thermophoresis on Williams on Nano Fluid Flow Past a Stretching Sheet: MHD and Chemical Reaction Effects

Teku Lokesh Babu[1,*], Krishna Kumari Gannamaraju[2], Mamidi Narsimha Rajashekar[3]

[1] Department of Mathematics, Sreenidhi Institute of Science and Technology, Hyderabad, Telangana, India
[2] Department of Mathematics, Vardhaman College of Engineering, Hyderabad, Telangana, India
[3] Department of Mathematics, College of Engineering, JNT University, Hyderabad, Telangana, India

ARTICLE INFO

Article history:
Received 13 April 2024
Received in revised form 12 July 2024
Accepted 20 July 2024
Available online 15 August 2024

Keywords:
Nanofluid; Williamson fluid; magnetic field; Thermophoresis; Brownian motion; stretching sheet; chemical reaction; finite element method

ABSTRACT

The objective of this study is to numerically solve the Williamson fluid flow equations across a non-linear stretching sheet while taking into account the existence of nanofluid particles, the effect of a magnetic field, and the impact of a chemical reaction. The energy and concentration equations account for the effects of thermophoresis and Brownian motion. The finite element approach is used to resolve the governing nonlinear equations of the fluid flow and the associated boundary conditions. Through graphical representations, the research explores the effects of several pertinent factors on the profiles of concentration, temperature, and velocity. Also shown in tabular form are the impacts of these factors on the skin-friction coefficient, Nusselt and Sherwood numbers, and heat and mass transfer rates. The correctness of the numerical model utilised in this research is then validated by comparison of the generated results with earlier findings.

1. Introduction

The Finite Element Method (FEM) is a potent numerical technique used to solve partial differential equations (PDEs) in engineering and applied sciences. In conjunction with nano fluid research, the Finite Element Method (FEM) permits the investigation of heat transfer and fluid dynamics in systems that contain nano particles dispersed in a host fluid. Nanofluids are colloidal suspensions of nanoparticles with diameters typically ranging from 1 to 100 nano-meters that are dispersed in a base fluid. Nanoparticles added to a base fluid can substantially alter its thermodynamic and flow characteristics, resulting in increased heat transfer rates and anomalous fluid dynamics. To incorporate nanofluids into the finite element method (FEM), the governing equations for fluid flow and heat transfer must be modified to account for the presence of nanoparticles. The addition of additional elements to the conservation equations for mass, momentum, and energy accounts for the effects of nano particle motion, interfacial interactions, and

* *Corresponding author.*
E-mail address: lokeshbabutekut@sreenidhi.edu.in

https://doi.org/10.37934/arfmts.120.1.6884

increases in thermal conductivity. The Finite Element Method (FEM) uses suitable basis functions to discretize the computational domain into finite elements, allowing for the estimation of solution variables for velocity, pressure, temperature, and nanoparticle concentration. The fundamental operations were chosen to represent the essential properties of thermal transfer and fluid movement in nano fluids. The FEM then assembles the fundamental equations into a comprehensive system of equations, after which it numerically resolves the fields of velocity, pressure, temperature, and nanoparticle concentration within the domain. Several numerical methods, including the Newton-Raphson method, can be used to resolve the equations' nonlinearities. The Finite Element Method (FEM) can be used to investigate a variety of nanofluid phenomena, such as forced convection, natural convection, and heat transfer enhancement in channels or pipelines with complex geometries. This methodology enables the investigation of the effects of multiple variables on the characteristics of fluid dynamics and thermal energy exchange, including the concentration, dimensions, and physical properties of nanoscale particles. The use of the Finite Element Method (FEM) in conjunction with nanofluids can aid in the comprehension of nanofluid systems' behaviour, improve heat transfer efficiency, and establish effective thermal management solutions for a variety of applications, including but not limited to electronics cooling, energy systems, and biomedical applications. This strategy can be especially useful for engineers and scientists. Sabour *et al.,* [1] studied natural convection of nanofluids in a cavity. Brinkman [2] discussed viscosity in highly concentrated solutions and suspensions. Chon *et al.,* [3] presented an empirical correlation that investigates the impact of particle size and temperature on the enhancement of thermal conductivity in nanofluids. Duangthongsuk and Wongwises [4] aimed to obtain experimental data on the temperature-dependent thermal conductivity and viscosity of TiO_2-water nanofluids as their primary objective. Ghasemi and Aminossadati [5] studied Brownian motion of nanoparticles in a triangular enclosure with natural convection. In a study conducted by Khanafer *et al.,* [6], the use of nanofluids for enhancing buoyancy-driven heat transmission within a two-dimensional container was investigated. Kuznetsov and Nield [7] studied the flow of a nanofluid over a vertical plate, concentrating explicitly on the natural convective boundary-layer. According to their publication from Mahian *et al.,* [8], conducted a study on the use of nanofluids in solar energy systems. Nguyen *et al.,* [9] studied Heat transfer enhancement using Al2O3-water nanofluid for an electronic liquid cooling system. Nguyen *et al.,* [10] studied temperature and particle-size dependent viscosity data for water-based nanofluids–hysteresis phenomenon. Oztop and Abu-Nada [11] studied natural convection in partially heated rectangular enclosures filled with nanofluids using numerical solutions. Tiwari and Das [12] studied heat transfer augmentation in a two-sided lid-driven differentially heated square cavity utilizing nanofluids. Maheswari *et al.,* [13] studied MHD forchheimer flow of Fe_3O_4−H_2O, Cu−H_2O and Ag−H_2O nanofluids over permeable stretching sheet with radiation. Guled *et al.,* [14] studied the heat transfer effects of MHD slip flow with suction and injection and radiation over a shrinking sheet by optimal homotopy analysis method. Dharmaiah *et al.,* [15] discussed the performance of magnetic dipole contribution on ferromagnetic non-Newtonian radiative MHD blood flow. Manvi *et al.,* [16] studied the effects of MHD radiating and non-uniform heat source/sink with heating on the momentum and heat transfer of Eyring-Powell fluid over a stretching. Arulmozhi *et al.,* [17] discussed heat and mass transfer analysis of radiative and chemical reactive effects on MHD nanofluid over an infinite moving vertical plate. Several researchers have investigated the properties of nanofluids [18-30].

In the context of a chemical reaction, the reference works have inspired research into the effects of thermophoresis, Brownian motion, and a magnetic field on the characteristics of nanofluid flow over a stretched sheet. The use of Williamson fluid is widespread in the simulation of nanofluid, as it effectively represents the non-Newtonian properties of the fluid. The study utilised the finite element

method to solve the governing equations for the issue at hand. The purpose of this investigation is to determine the effect of Thermophoretic and Brownian forces, Magnetic field intensity, and Chemical reaction rate on the Velocity, Temperature, and Concentration profiles. The findings provide novel and important insights into the collective effects of magnetic field, Brownian motion, and thermophoresis. This research contributes to the comprehension of nanofluid flow and transport phenomena and has practical implications for a variety of engineering and industrial operations.

2. Mathematical Analysis

The combined effects of thermophoresis, magnetic field, and Brownian motion are investigated in this work on an incompressible, electrically conducting, viscous, 2D-steady, Williamson-Nanofluid flow towards a non-linear stretching sheet. Physical coordinates for this fluid route are shown in Figure 1. For the purpose of this endeavour, the ensuing speculations are analyzed.

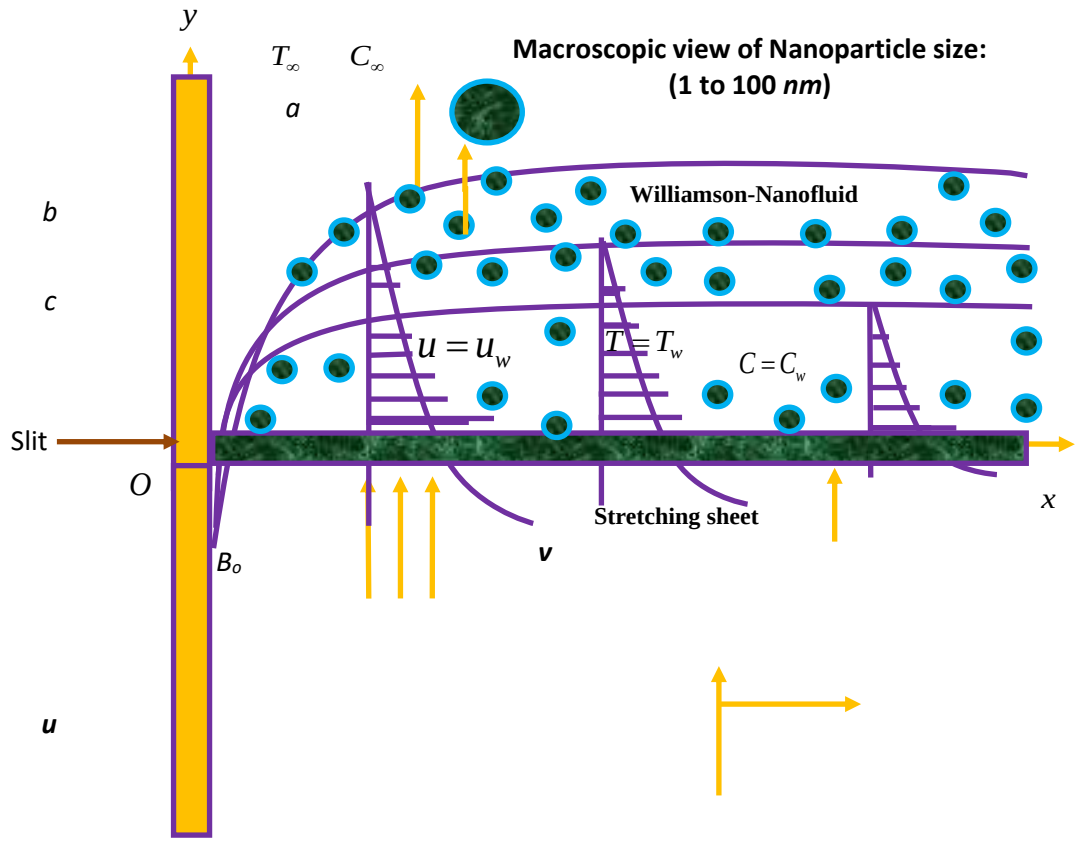

a ---- Momentum boundarylayer ***b*** ---- Thermal boundarylayer *c* ---- Concentration boundarylayer

Fig. 1. Physical coordinate representation of Williamson-Nanofluid

Let us consider the flow of a nanofluid through a stretching sheet that coincides with the plane $y = 0$ and is restricted to the region $y > 0$.

The flow is generated, due to non-linear stretching of the sheet, caused by the simultaneous application of two equal and opposite forces along the *x*-axis.

Normally, a variable magnetic field *B*(*x*) will be provided to the surface of the sheet while the magnetic field induced is minimal and may be justified for MHD flow at the small magnetic Reynolds number. It is assumed that the pressure gradient and external forces are ignored.

When the origin is held constant, the sheet is then stretched with a velocity $u_w = ax^n$, which varies non-linearly with distance from the slit.

The fluid temperature and concentration of the stretching surface, T_w and C_w, are kept at constant values, and these values are considered to be higher than the temperature and concentration of the surrounding environment, T_∞ and C_∞, which are maintained at constant values.

Based on the above assumptions, the basic mass, momentum, energy, and nanoparticles equations for Williamson-Nanofluids can be written as

Continuity Equation

$$\left(\frac{\partial u}{\partial x}\right)+\left(\frac{\partial v}{\partial y}\right)=0 \tag{1}$$

Momentum Equation

$$u\frac{\partial u}{\partial x}+v\frac{\partial u}{\partial y}=\nu\left(\frac{\partial^2 u}{\partial y^2}\right)+\sqrt{2}\Gamma\left[\frac{\partial u}{\partial y}\right]\left[\frac{\partial^2 u}{\partial y^2}\right]-\left(\frac{\sigma B_o^2}{\rho}\right)u, \tag{2}$$

Equation of thermal energy

$$u\frac{\partial T}{\partial x}+v\frac{\partial T}{\partial y}=\alpha\left(\frac{\partial^2 T}{\partial y^2}\right)+\tau_B\left\{D_B\left[\frac{\partial C}{\partial y}\frac{\partial T}{\partial y}\right]+\frac{D_T}{T_\infty}\left(\frac{\partial T}{\partial y}\right)^2\right\} \tag{3}$$

Equation of nanoparticle concentration

$$u\left(\frac{\partial C}{\partial x}\right)+v\left(\frac{\partial C}{\partial y}\right)=D_B\left(\frac{\partial^2 C}{\partial y^2}\right)+\left(\frac{D_T}{T_\infty}\right)\left(\frac{\partial^2 T}{\partial y^2}\right)-Kr\left(C-C_\infty\right) \tag{4}$$

Subject to the boundary conditions for Williamson-nanofluid flow are

$$\left.\begin{aligned} &u=u_w=ax^n,\ v=0,\ T=T_w,\ C=C_w\ at\ \ y=0\\ &u\to 0,\ v\to 0,\ T\to T_\infty,\ C\to C_\infty\ as\ \ y\to\infty \end{aligned}\right\} \tag{5}$$

The following similarity variables are introduced for solving governing Eq. (2) to Eq. (4) as

$$\left.\begin{aligned} &\eta=y\left(\sqrt{\frac{a(n+1)}{2\nu}}\right)x^{\frac{n-1}{2}},\ u=ax^n f'(\eta),\ v=-\left(\sqrt{\frac{a\nu(n+1)}{2}}\right)x^{\frac{n-1}{2}}\left(f(\eta)+\left(\frac{n-1}{n+1}\right)\eta f'(\eta)\right),\\ &\theta(\eta)=\frac{T-T_\infty}{T_w-T_\infty},\ \phi(\eta)=\frac{C-C_\infty}{C_w-C_\infty} \end{aligned}\right\} \tag{6}$$

Using Eq. (6), the fundamental Eq. (2) to Eq. (4) become

$$f''' + ff'' - \left(\frac{2n}{n+1}\right) f'^2 - Mf' + \lambda f'' f''' = 0 \tag{7}$$

$$\theta'' + \Pr f\theta' + \Pr Nb\theta'\phi' + \Pr Nt\theta'^2 = 0 \tag{8}$$

$$2Nb\phi'' + NbLef\phi' + 2Nt\theta'' - 2\gamma Nb\phi = 0 \tag{9}$$

and the corresponding boundary conditions (5) become

$$\left.\begin{array}{l} f = 0, \quad f' = 1, \quad \theta = 1, \quad \phi = 1 \quad at \quad \eta = 0 \\ f' \to 0, \quad \theta \to 0, \quad \phi \to 0 \quad as \quad \eta \to \infty \end{array}\right\} \tag{10}$$

where the involved physical parameters are defined as

$$\left.\begin{array}{l} \Pr = \dfrac{\nu}{\alpha},\ M = \dfrac{\sigma B_o^2 x}{\rho a},\ Le = \dfrac{\nu}{D_B},\ Nb = \dfrac{\left(\rho C\right)_p D_B (C_w - C_\infty)}{\left(\rho C\right)_f \nu}, \\ \lambda = \Gamma x\sqrt{\dfrac{2a^3}{\nu}},\quad Nt = \dfrac{\left(\rho C\right)_p D_T (T_w - T_\infty)}{\left(\rho C\right)_f \nu T_\infty},\ \gamma = \dfrac{Kr}{a} \end{array}\right\} \tag{11}$$

The parameters of engineering interest in heat and mass transport problems are the Skin-friction coefficient $\left(Cf\right)$, local Nusselt number $\left(Nu_x\right)$ and the Sherwood number $\left(Sh_x\right)$ are defined as

$$Cf = \frac{\tau_w}{\rho u_w^2} = \frac{\mu}{\rho u_w^2}\left(\frac{\partial u}{\partial y} + \frac{\Gamma}{\sqrt{2}}\left(\frac{\partial u}{\partial y}\right)^2\right)_{y=0} \Rightarrow \left(\sqrt{\mathrm{Re}_x}\right) Cf = f''(0)\left(1 + \frac{\lambda}{2} f''(0)\right) \tag{12}$$

$$Nu_x = \frac{xq_w}{\kappa\left(T_w - T_\infty\right)} \text{ where } q_w = -\kappa\left(T_w - T_\infty\right) x^{\frac{n-1}{2}} \left(\sqrt{\frac{a\left(n+1\right)}{2\nu}}\right)\theta'(0)$$

$$\Rightarrow Nu_x = -x^{\frac{n+1}{2}} \left(\sqrt{\frac{a\left(n+1\right)}{2\nu}}\right)\theta'(0) \tag{13}$$

$$Sh_x = \frac{xq_m}{D_B\left(C_w - C_\infty\right)} \text{ where } q_m = -D_B\left(C_w - C_\infty\right) x^{\frac{n-1}{2}} \left(\sqrt{\frac{a\left(n+1\right)}{2\nu}}\right)\phi'(0)$$

$$\Rightarrow Sh_x = -x^{\frac{n+1}{2}} \left(\sqrt{\frac{a\left(n+1\right)}{2\nu}}\right)\phi'(0) \tag{14}$$

3. Numerical Solutions by Finite Element Method

In this section, we have to find the numerical solutions of ordinary differential equations (7), (8) and (9) with the help of boundary conditions (10) using finite element method. The structure of finite element method is as shown in Figure 2.

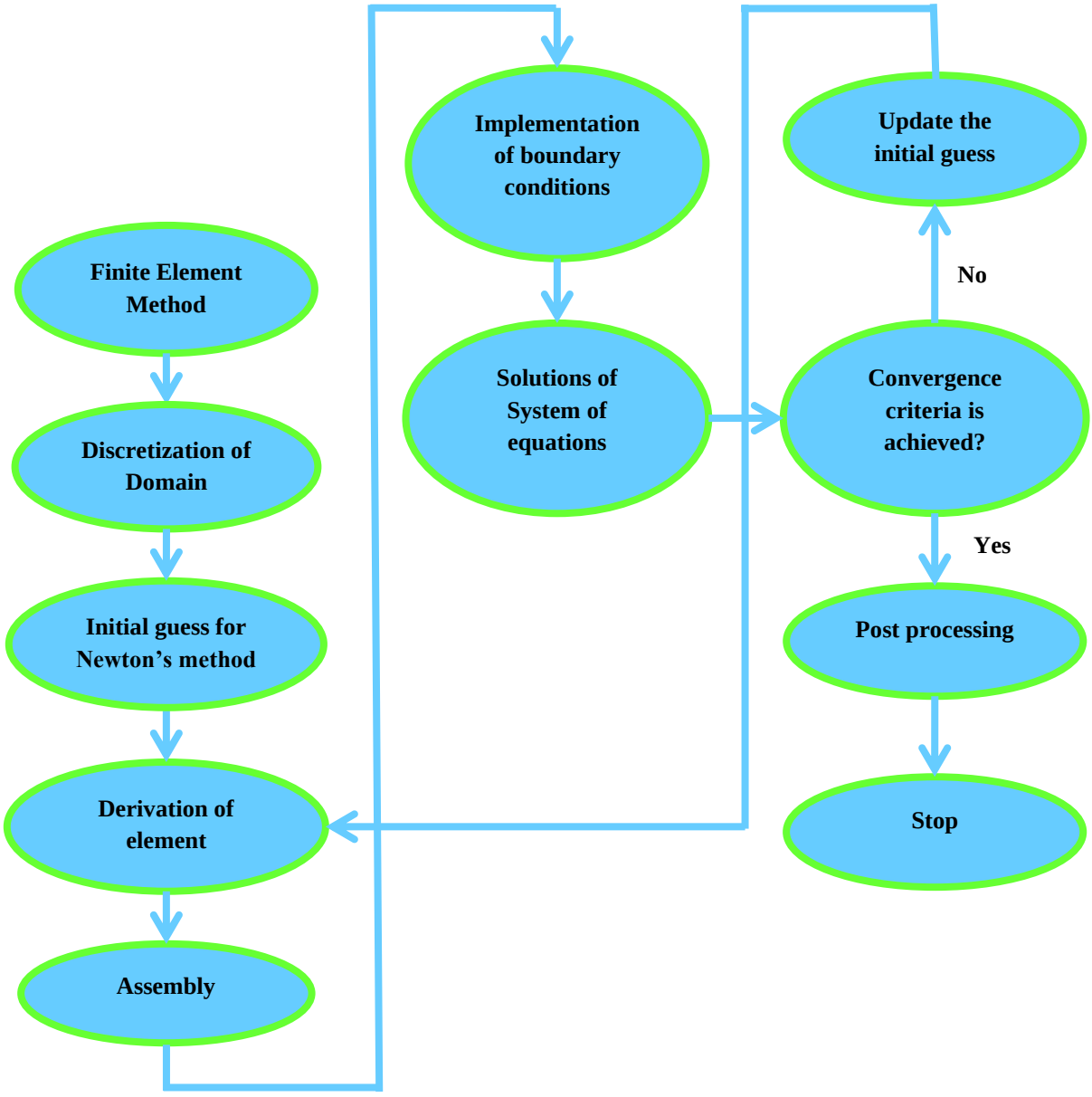

Fig. 2. Flow chart of Finite Element Method

3.1 Finite Element Modelling

Details of method used here are available in the work by Reddy [31]. Figure 2 elaborates the finite-element modelling stages. To solve Eq. (7), Eq. (8), Eq. (9) considering Eq. (10), assume

$$f' = h \tag{15}$$

The system of equations get reduces to

$$h'' + fh' - \left(\frac{2n}{n+1}\right)h^2 - Mh + \lambda h' h'' = 0 \tag{16}$$

$$\theta'' + \Pr\, f\theta' + \Pr Nb\theta'\phi' + \Pr Nt\theta'^2 = 0 \tag{17}$$

$$2Nb\phi'' + NbLef\phi' + 2Nt\theta'' - 2\gamma Nb\phi = 0 \tag{18}$$

with $\left.\begin{array}{l} f = 0,\ \ h = 1,\ \ \theta = 1,\ \ \phi = 1 \ \ at \ \ \eta = 0 \\ h \to 0,\ \ \theta \to 0,\ \ \ \phi \to 0 \ \ as \ \ \eta \to \infty \end{array}\right\}$ (19)

3.2 Variational Form

Over element $(\eta_e,\ \eta_{e+1})$, variational form linked with Eq. (16) to Eq. (18) is

$$\int_{\eta_e}^{\eta_{e+1}} w_1 \left(f' - h \right) d\eta = 0 \tag{20}$$

$$\int_{\eta_e}^{\eta_{e+1}} w_2 \left(h'' + fh' - \left(\frac{2n}{n+1}\right)h^2 - Mh + \lambda h' h'' \right) d\eta = 0 \tag{21}$$

$$\int_{\eta_e}^{\eta_{e+1}} w_3 \left(\theta'' + \Pr\, f\theta' + \Pr Nb\theta'\phi' + \Pr Nt\theta'^2 \right) d\eta = 0 \tag{22}$$

$$\int_{\eta_e}^{\eta_{e+1}} w_4 \left(2Nb\phi'' + NbLef\phi' + 2Nt\theta'' - 2\gamma Nb\phi \right) d\eta = 0 \tag{23}$$

Here, w_1, w_2, w_3 and w_4 are linearly independent functions known as weight functions in relation to variation in f, f', ϑ and ϕ respectively.

3.3 Finite Element Form

Considering $w_1 = w_2 = w_3 = w_4 = \psi_i$ and

$$f = \sum_{j=1}^{2} (f)_j \psi_j,\ \ h = \sum_{j=1}^{2} (h)_j \psi_j,\ \ \theta = \sum_{j=1}^{2} (\theta)_j \psi_j,\ \ \phi = \sum_{j=1}^{2} (\phi)_j \psi_j, \tag{24}$$

with linear interpolation functions

$\psi_1 = (\eta_{e+1} - \eta_e)^{-1} (\eta_{e+1} - \eta)$ and $\psi_2 = (\eta_{e+1} - \eta_e)^{-1} (\eta - \eta_e)$, $\eta_e \le \eta \le \eta_{e+1}$

along with quadratic interpolation functions

$$\psi_1 = (\eta_{e+1} + \eta_e - 2\eta)(\eta_{e+1} - \eta)(\eta_{e+1} - \eta_e)^{-2},$$

$$\psi_2 = 4(\eta - \eta_e)(\eta_{e+1} - \eta)(\eta_{e+1} - \eta_e)^{-2},$$

and $\psi_3 = (\eta_{e+1} + \eta_e - 2\eta)(\eta - \eta_e)(\eta_{e+1} - \eta_e)^{-2}$

we obtain the finite element model after substituting Eq. (24) into Eq. (20) to Eq. (23) as

$$\begin{Bmatrix} [K^{11}] & [K^{12}] & [K^{13}] & [K^{14}] \\ [K^{21}] & [K^{22}] & [K^{23}] & [K^{24}] \\ [K^{31}] & [K^{32}] & [K^{33}] & [K^{34}] \\ [K^{41}] & [K^{42}] & [K^{43}] & [K^{44}] \end{Bmatrix} \begin{Bmatrix} \{f\} \\ \{h\} \\ \{\theta\} \\ \{\phi\} \end{Bmatrix} = \begin{Bmatrix} \{r^1\} \\ \{r^2\} \\ \{r^3\} \\ \{r^4\} \end{Bmatrix} \tag{25}$$

Here $[K^{mn}]$ and $\{r^m\}$ are 2×2 and 2×1 order matrices (m, n = 1, 2, 3, 4) respectively, where

$$K_{ij}^{11} = \int_{\eta_e}^{\eta_{e+1}} \psi_i \frac{d\psi_j}{d\eta} d\eta, \quad K_{ij}^{12} = -\int_{\eta_e}^{\eta_{e+1}} \psi_i \psi_j d\eta,$$

$$K_{ij}^{22} = \int_{\eta_e}^{\eta_{e+1}} \frac{d\psi_i}{d\eta}\frac{d\psi_j}{d\eta} d\eta + \int_{\eta_e}^{\eta_{e+1}} \psi_i \frac{d\psi_j}{d\eta} d\eta - \left(\frac{2n}{n+1}\right)\int_{\eta_e}^{\eta_{e+1}} \bar{h}\psi_i\psi_j d\eta - M\int_{\eta_e}^{\eta_{e+1}} \psi_i\psi_j d\eta + \lambda\int_{\eta_e}^{\eta_{e+1}} \frac{d\psi_i}{d\eta}\frac{d\psi_j}{d\eta} d\eta,$$

$$K_{ij}^{31} = K_{ij}^{32} = K_{ij}^{34} = 0, \quad K_{ij}^{41} = K_{ij}^{42} = K_{ij}^{43} = 0, \quad K_{ij}^{13} = K_{ij}^{14} = 0, \quad K_{ij}^{21} = K_{ij}^{23} = K_{ij}^{24} = 0,$$

$$K_{ij}^{33} = \int_{\eta_e}^{\eta_{e+1}} \frac{d\psi_i}{d\eta}\frac{d\psi_j}{d\eta} d\eta + \Pr\int_{\eta_e}^{\eta_{e+1}} \psi_i \frac{d\psi_j}{d\eta} d\eta + \Pr Nb\int_{\eta_e}^{\eta_{e+1}} \bar{h}\psi_i\psi_j d\eta + \Pr Nt\int_{\eta_e}^{\eta_{e+1}} \psi_i \frac{d\psi_j}{d\eta} d\eta,$$

$$K_{ij}^{44} = 2Nb\int_{\eta_e}^{\eta_{e+1}} \frac{d\psi_i}{d\eta}\frac{d\psi_j}{d\eta} d\eta + NbLe\int_{\eta_e}^{\eta_{e+1}} \psi_i \frac{d\psi_j}{d\eta} d\eta + 2Nt\int_{\eta_e}^{\eta_{e+1}} \bar{h}\psi_i\psi_j d\eta - 2\gamma Nb\int_{\eta_e}^{\eta_{e+1}} \psi_i\psi_j d\eta,$$

$$r_i^1 = 0, \quad r_i^2 = -M\int_{\eta_e}^{\eta_{e+1}} \psi_i d\eta - \left[\psi_i \frac{dh}{d\eta}\right]_{\eta_e}^{\eta_{e+1}}, \quad r_i^3 = -\frac{1}{\Pr}\left[\psi_i \frac{d\theta}{d\eta}\right]_{\eta_e}^{\eta_{e+1}}, \quad r_i^4 = -\frac{1}{Sc}\left[\psi_i \frac{d\phi}{d\eta}\right]_{\eta_e}^{\eta_{e+1}},$$

and $\bar{f} = \sum_{i=1}^{2} \bar{f}_i\psi_i, \ \bar{h} = \sum_{i=1}^{2} \bar{h}_i\psi_i$ assumed to be known.

No significant change in the results has been observed for large values of η (> 4). Thus, without loss of generality for the computational purposes, ∞ can be fixed at 4. The total domain is split into *n*-linear elements having width $h_e\left(=\eta_{e+1}-\eta_e\right)$ where $h_e = 4/n$ and *n* = 1000. After assembling all element equations, we get matrix of order 4004. New system obtained is highly nonlinear and linearized by incorporating the function $\bar{f}$, $\bar{h}$. By sustaining an accuracy of 0.000001, an iterative scheme for *f*, *h*, ϑ and ϕ is employed to solve remaining system of equations. Linear, quadratic, and higher order interpolation functions can be used for 1-D and 2-D problems. Though, fitness of interpolation function differs with the problem, linear and quadratic interpolation functions are utilised owing to simple and effective usage in computations.

4. Code Validation

The current rate of heat transfer results is compared to the previously published rate of heat transfer number results of Cortell [32] in Table 1 in the absence of Magnetic field, Williamson fluid, thermophoresis, Brownian motion, and Chemical reaction for code validation of current numerical results. As can be seen in this table, the present numerical findings are in perfect agreement with the results that have been published. This shows that there is a lot of agreement between the two research, which gives the current study a lot of confidence. This gives our numerical findings validity.

Table 1
Assessment of current rate of heat transfer results with the published results

Pr	*n*	Nusselt number results of Cortell [32]	Present Nusselt number results
1.0	0.2	0.610262	0.5943986793893
	0.5	0.595277	0.5856470629727
	1.5	0.574537	0.5697819854984
	3.0	0.564472	0.5515675262398
	10.0	0.554960	0.5486728068472
5.0	0.2	1.607175	1.5867168953481
	0.5	1.586744	1.5615073481066
	1.5	1.557463	1.5476771796312
	3.0	1.542337	1.5288758717430
	10.0	1.528573	1.5187717389921

5. Results and Discussion

The finite element approach is being used in the current study to explore the impacts of Brownian motion and thermophoresis on Williamson-Nanofluid flow via a stretched sheet with the influence of chemical reaction and magnetic field. Figure 3 to Figure 12 show the effects of various emerging parameters on the velocity profiles, temperature distribution, and concentration profiles of Williamson-Nanofluid. These parameters include the Magnetic field parameter (*M*), Williamson fluid parameter (λ), Stretching sheet parameter (*n*), Prandtl number (Pr), Thermophoresis parameter (*Nt*), Brownian motion parameter (*Nb*), Lewis number (*Le*), and Chemical reaction parameter (γ), and the arithmetic values of Skin-friction coefficient, Nusselt number and Sherwood number are presented in Table 2, Table 3 and Table 4. It is unchanging *M* = 0.3, λ = 0.5, *n* = 0.3, Pr = 0.71, *Nb* = 0.3, *Nt* = 0.1, *Le* = 0.3, and γ = 0.5.

Figure 3 illustrates that when the Magnetic field parameter (*M*) is increased, the velocity profile diminishes due to the retarding force, which causes the velocity to decrease. Due to its resistive character, the magnetic field parameter *M* induces the Lorentz force, which reduces the velocity of

the fluid. The impact of a change in the Williamson fluid parameter (Weissenberg number (λ)) on velocity profiles is shown in Figure 4. The study of viscoelastic flows makes use of the dimensionless Williamson fluid parameter. It bears Karl Weissenberg's name. The viscous and elastic forces are contrasted in this number. This value λ, which contains choices for the length scale, shear or elongation rate, and stress evolution scaling, is obtained. It is seen that as the velocity increases, the vertical component of the velocity distribution decreases. This assertion is supported by the observation that when the fluid's relaxation time grows, the Weissenberg number λ also does, increasing flow resistance and boundary layer thickness.

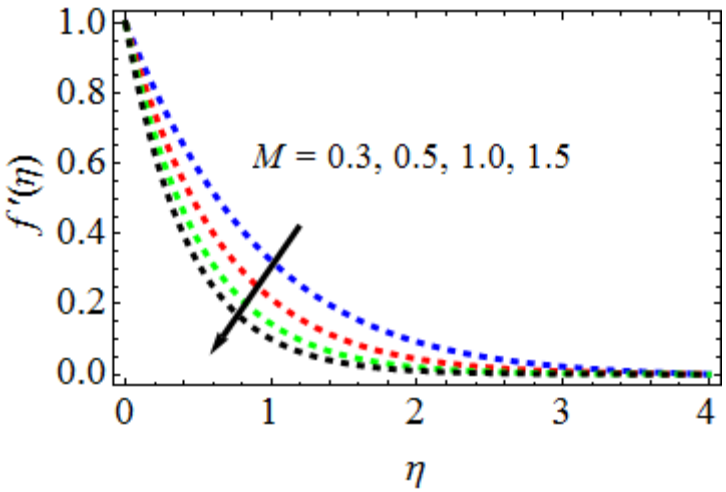

Fig. 3. Features of *M* on velocity profiles

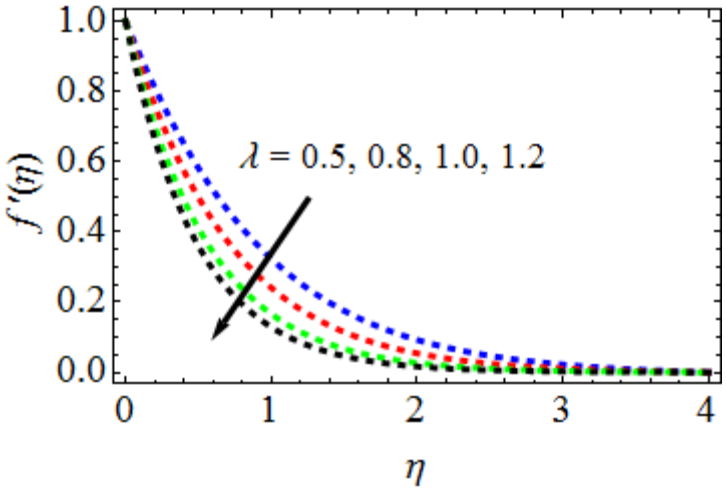

Fig. 4. Features of λ on velocity profiles

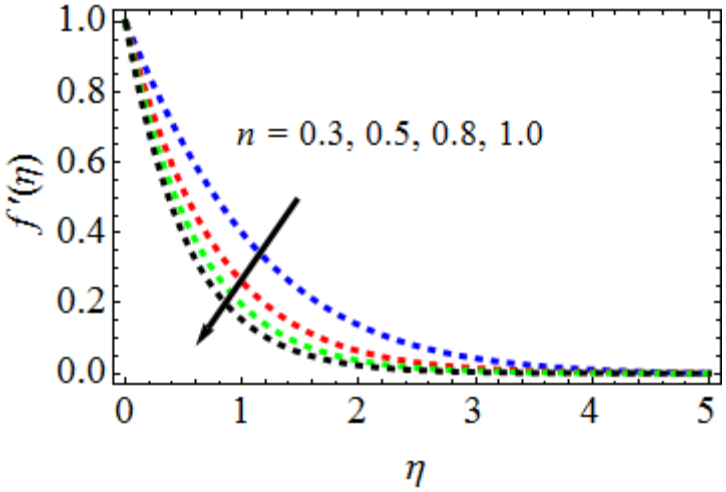

Fig. 5. Features of *n* on velocity profiles

The velocity profiles in Figure 5 illustrate how the values of the stretching parameter (*n*) vary for various non-linear stretching parameters. The conclusion that can be derived from this observation is that the velocity profiles become flatter as *n* increases. In other words, as the non-linear stretching parameter *n* is increased, the thickness of the momentum barrier layer will decrease. The temperature shift brought on by the fluid's Prandtl number (Pr) is seen in Figure 6. The fluid's temperature gradient becomes less noticeable as Pr rises. The graph below demonstrates that when Pr grows, the momentum diffusivity increases while the thermal diffusivity becomes less relevant. It is necessary for the fluid velocity to be sufficiently high for heat transfer to occur. This process causes a reduction in boundary layer thickness and an acceleration in the rate of heat dissipation.

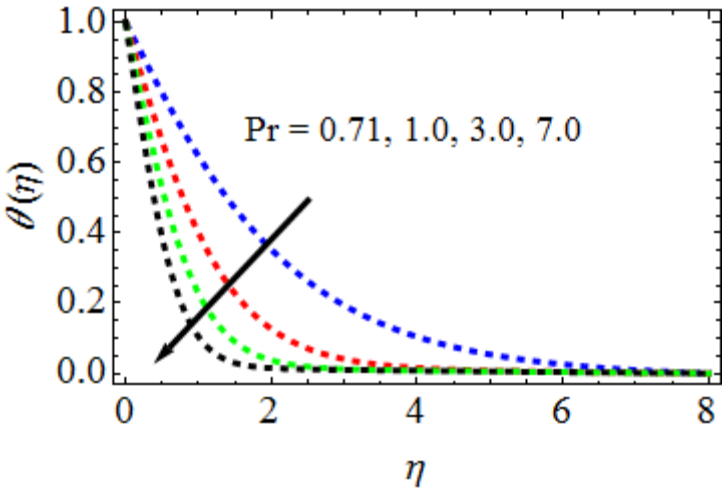

Fig. 6. Features of Pr on temperature profiles

Figure 7 and Figure 8 depict, respectively, the effect of the Brownian motion parameter (*Nb*) on the temperature (ϑ) and concentration (ϕ) profiles. Temperature profiles rise as Brownian motion parameter values increase, but concentration profiles experience the opposite trend. The thickness of the boundary layer is proportional to the temperature of the nanofluid as a function of *Nb*. It occurs as a result of the nanoscale particles increased kinetic energy enhancing their chaotic motion. In addition, the effect of Brownian motion on focus becomes less pronounced as the nanoparticle motion becomes increasingly chaotic.

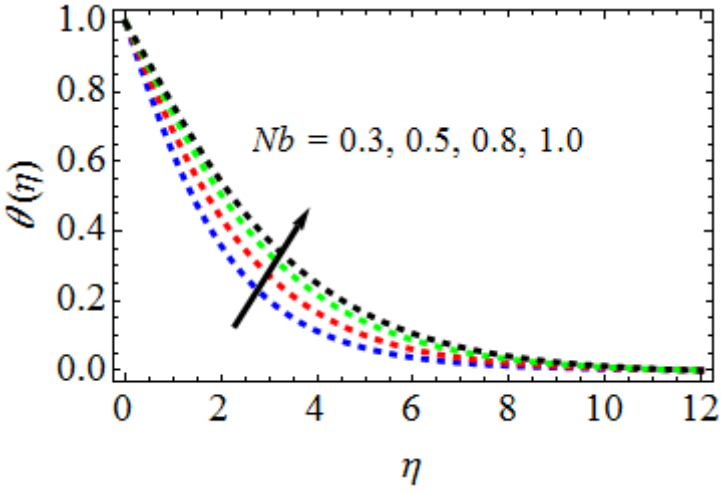

Fig. 7. Features of *Nb* on temperature profiles

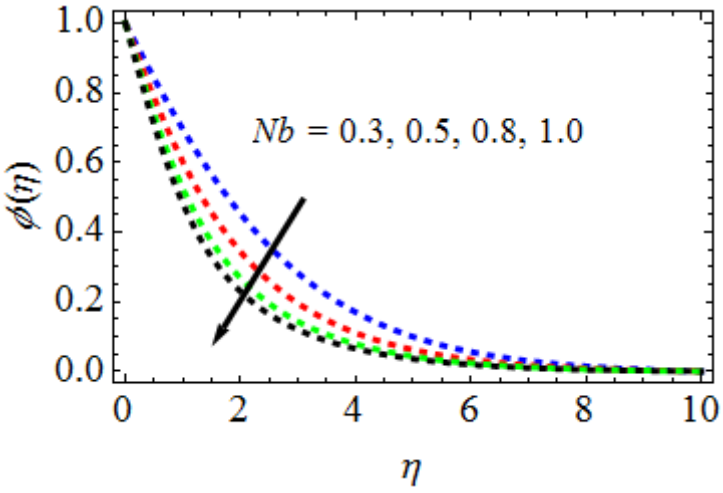

Fig. 8. Features of *Nb* on concentration profiles

The difference of Thermophoresis parameter (*Nt*) on temperature (ϑ) and concentration (ϕ) profiles can be seen via Figure 9 and Figure 10 respectively. It is observed that both temperature profiles and nanoparticle concentration profiles and their boundarylayer thicknesses are moving functions of approximated parameter *Nt*. Also, concentration overshoot is observed for higher *Nt*. Thermophoresis force is a temperature gradient force that causes transportation of hotter molecules having more kinetic energy towards the low temperature region. Therefore, the nanoparticle concentration and fluid temperature increase with the thermophoretic force. The relationship between the nanofluid Lewis number (*Le*) and nanoparticle concentration is depicted in Figure 11. This number is known as the Lewis number, and it quantifies the amount of heat and mass that a nanofluid without dimensions can diffuse. As Le's value increases, the fraction of nanoparticle volume decreases substantially. Figure 12 shows how the chemical reaction parameter (γ) affects concentration profiles. The thickness of the border layer of the concentration profile decreases with increasing size. As a result, concentration profiles become less intense. Additionally, it is noted that the solute boundary layer thickness decreases as the chemical reaction parameter γ rises. This is only because the molecule diffusivity reduces with increasing chemical reaction parameter values, which lowers fluid concentration.

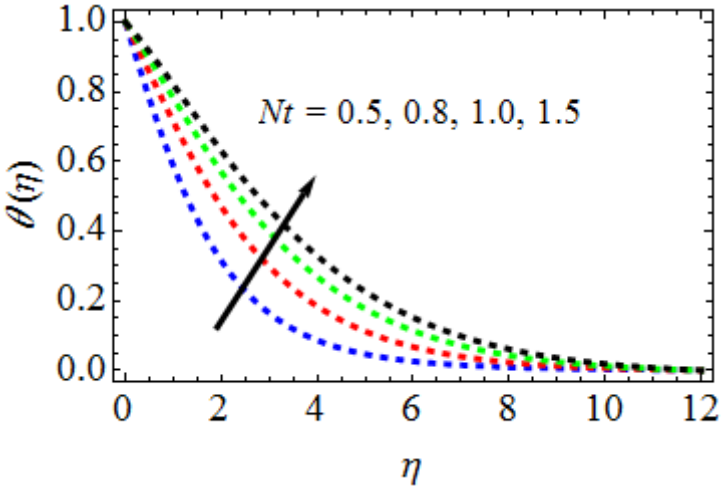

Fig. 9. Features of *Nt* on temperature profiles

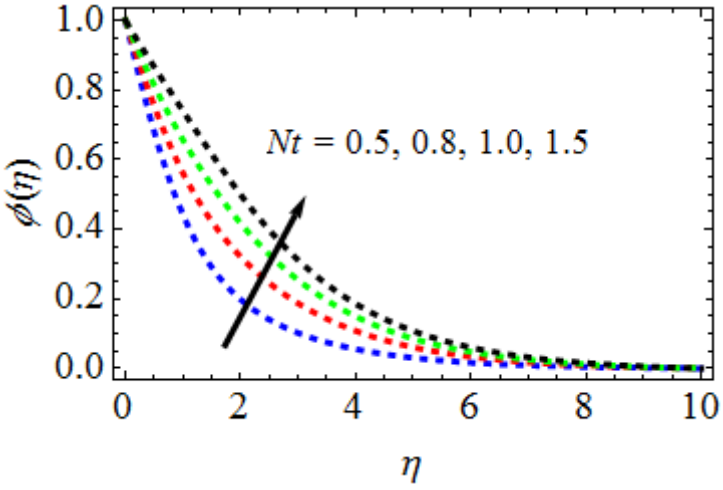

Fig. 10. Features of *Nt* on concentration profiles

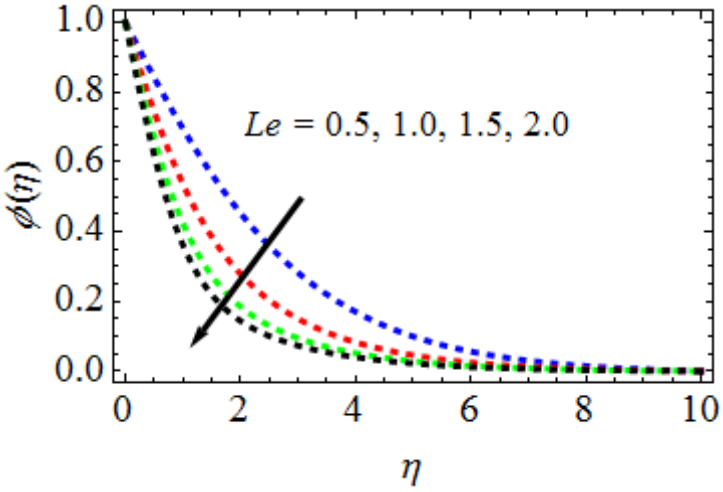

Fig. 11. Features of *Le* on concentration profiles

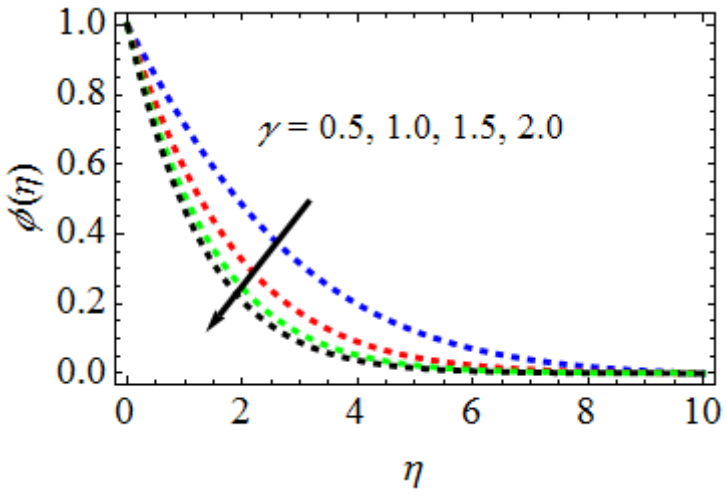

Fig. 12. Features of *γ* on concentration profiles

Table 2 shows the numerical values of Skin-friction coefficient for variations in values of the engineering parameters such as, *n*, *M*, *λ*, Pr, *Nt*, *Nb*, *γ*, and *Le*. From this table, it is observed that the Skin-friction coefficient is increasing with rising values of *Nt*, *Nb*, while it is decreasing with increasing values of *n*, *M*, *λ*, Pr, *γ* and *Le*. The numerical values of rate of heat transfer coefficient in terms of Nusselt number are displayed in Table 3 for different values of Pr, *Nt*, *Nb*. The rate of heat transfer coefficient is gradually rising with increasing values of *Nt*, *Nb*, while the reverse effect is observed in increasing values of Pr. The effects of *Nt*, *Nb*, *γ*, and *Le* on rate of mass transfer coefficient or in terms Sherwood number coefficient are discussed in Table 4. From this table, it is observed that the rate of mass transfer coefficient is increasing with increasing values of *Nt*, while it decreasing with increasing values of *Nb*, *γ*, and *Le*.

Table 2
Skin-friction coefficient numerical values

n	*M*	Pr	*Nt*	*Nb*	*γ*	*Le*	*λ*	*Cf*
0.3	0.3	0.71	0.5	0.3	0.5	0.3	0.5	1.7867437739479
0.5								1.7467896457318
0.8								1.7278819864564
	0.5							1.7500006714983
	1.0							1.7367583973939
		1.00						1.7409348693394
		3.00						1.7194776413473
			0.8					1.8177890198983
			1.0					1.8301095676852
				0.5				1.8045738734384
				0.8				1.7834376678735
					1.0			1.7538748734818
					1.5			1.7367637634076
						0.5		1.7415786188721
						0.8		1.7294731648738
							0.8	1.7567178387343
							1.0	1.7276671376097

Table 3
Rate of heat transfer coefficient numerical values

Pr	*Nt*	*Nb*	Nu_x
0.71	0.5	0.3	1.1267883963398
1.00			1.0856476876733
3.00			1.0401947587321
	0.8		1.1624287458974
	1.0		1.1808087138769
		0.5	1.1578688985596
		0.8	1.1755469639410

Table 4
Rate of mass transfer coefficient numerical values

Le	*Nt*	*Nb*	*γ*	Sh_x
0.3	0.5	0.3	0.5	1.3467673690342
0.5				1.3067671606387
0.8				1.2895648768728
	0.8			1.3712356956639
	1.0			1.3967678973891
		0.5		1.3167993169380
		0.8		1.2968793487981
			1.0	1.3074317963904
			1.5	1.2778718869343

6. Conclusions

This research looks at how a Magnetic field and Thermophoresis affect a continuous, two-dimensional Williamson-nanofluid flow across a stretched sheet that is electrically conducting, viscous, incompressible, and electrically conducting. using the finite element approach, the flow is controlled by basic nonlinear coupled ordinary differential equations. Profiles of flow variables like concentration, velocity, and temperature are examined using engineering considerations, and numerical data is produced as a consequence of the findings. The key facets of this inquiry are as follows

i. The velocity profiles decrease with rising values of *M*, *λ* and *n*.
ii. Temperature profiles increase for growing values of *Nt* and *Nb* parameters and decreases with increasing values of Pr.
iii. The concentration reduces with increasing in *Nb*, *γ* and *Le* and increasing with increasing values of *Nt*.
iv. In order to certify validity, the findings are also compared with earlier published results, which are found to be in reasonably good agreement.

References

[1] Sabour, M., Mohammad Ghalambaz, and Ali Chamkha. "Natural convection of nanofluids in a cavity: criteria for enhancement of nanofluids." *International Journal of Numerical Methods for Heat & Fluid Flow* 27, no. 7 (2017): 1504-1534. https://doi.org/10.1108/HFF-12-2015-0516

[2] Brinkman, Hendrik C. "The viscosity of concentrated suspensions and solutions." *The Journal of Chemical Physics* 20, no. 4 (1952): 571. https://doi.org/10.1063/1.1700493

[3] Chon, Chan Hee, Kenneth D. Kihm, Shin Pyo Lee, and Stephen U. S. Choi. "Empirical correlation finding the role of temperature and particle size for nanofluid (Al_2O_3) thermal conductivity enhancement." *Applied Physics Letters* 87, no. 15 (2005). https://doi.org/10.1063/1.2093936

[4] Duangthongsuk, Weerapun, and Somchai Wongwises. "Measurement of temperature-dependent thermal conductivity and viscosity of TiO_2-water nanofluids." *Experimental Thermal and Fluid Science* 33, no. 4 (2009): 706-714. https://doi.org/10.1016/j.expthermflusci.2009.01.005

[5] Ghasemi, B., and S. M. Aminossadati. "Brownian motion of nanoparticles in a triangular enclosure with natural convection." *International Journal of Thermal Sciences* 49, no. 6 (2010): 931-940. https://doi.org/10.1016/j.ijthermalsci.2009.12.017

[6] Khanafer, Khalil, Kambiz Vafai, and Marilyn Lightstone. "Buoyancy-driven heat transfer enhancement in a two-dimensional enclosure utilizing nanofluids." *International Journal of Heat and Mass Transfer* 46, no. 19 (2003): 3639-3653. https://doi.org/10.1016/S0017-9310(03)00156-X

[7] Kuznetsov, A. V., and D. A. Nield. "Natural convective boundary-layer flow of a nanofluid past a vertical plate." *International Journal of Thermal Sciences* 49, no. 2 (2010): 243-247. https://doi.org/10.1016/j.ijthermalsci.2009.07.015

[8] Mahian, Omid, Ali Kianifar, Soteris A. Kalogirou, Ioan Pop, and Somchai Wongwises. "A review of the applications of nanofluids in solar energy." *International Journal of Heat and Mass Transfer* 57, no. 2 (2013): 582-594. https://doi.org/10.1016/j.ijheatmasstransfer.2012.10.037

[9] Nguyen, Cong Tam, Gilles Roy, Christian Gauthier, and Nicolas Galanis. "Heat transfer enhancement using Al_2O_3–water nanofluid for an electronic liquid cooling system." *Applied Thermal Engineering* 27, no. 8-9 (2007): 1501-1506. https://doi.org/10.1016/j.applthermaleng.2006.09.028

[10] Nguyen, C. T., F. Desgranges, Gilles Roy, Nicolas Galanis, Thierry Maré, eaS Boucher, and H. Angue Mintsa. "Temperature and particle-size dependent viscosity data for water-based nanofluids–hysteresis phenomenon." *International Journal of Heat and Fluid Flow* 28, no. 6 (2007): 1492-1506. https://doi.org/10.1016/j.ijheatfluidflow.2007.02.004

[11] Oztop, Hakan F., and Eiyad Abu-Nada. "Numerical study of natural convection in partially heated rectangular enclosures filled with nanofluids." *International Journal of Heat and Fluid Flow* 29, no. 5 (2008): 1326-1336. https://doi.org/10.1016/j.ijheatfluidflow.2008.04.009

[12] Tiwari, Raj Kamal, and Manab Kumar Das. "Heat transfer augmentation in a two-sided lid-driven differentially heated square cavity utilizing nanofluids." *International Journal of Heat and Mass Transfer* 50, no. 9-10 (2007): 2002-2018. https://doi.org/10.1016/j.ijheatmasstransfer.2006.09.034

[13] Maheswari, Chundru, Ravuri Mohana Ramana, Shaik Mohiddin Shaw, G. Dharmaiah, and S. Noeiaghdam. "Numerical investigation on MHD forchheimer flow of Fe_3O_4–H_2O, Cu–H_2O and Ag–H_2O nanofluids over permeable stretching sheet with radiation." *Results in Engineering* 18 (2023): 101194.

[14] Guled, C. N., J. V. Tawade, P. Kumam, S. Noeiaghdam, I. Maharudrappa, S. M. Chithra, and V. Govindan. "The heat transfer effects of MHD slip flow with suction and injection and radiation over a shrinking sheet by optimal homotopy analysis method." *Results in Engineering* 18 (2023): 101173. https://doi.org/10.1016/j.rineng.2023.101173

[15] Dharmaiah, G., J. L. Rama Prasad, K. S. Balamurugan, I. Nurhidayat, Unai Fernandez-Gamiz, and Samad Noeiaghdam. "Performance of magnetic dipole contribution on ferromagnetic non-Newtonian radiative MHD blood flow: An application of biotechnology and medical sciences." *Heliyon* 9, no. 2 (2023). https://doi.org/10.1016/j.heliyon.2023.e13369

[16] Manvi, Bharatkumar, Jagadish Tawade, Mahadev Biradar, Samad Noeiaghdam, Unai Fernandez-Gamiz, and Vediyappan Govindan. "The effects of MHD radiating and non-uniform heat source/sink with heating on the momentum and heat transfer of Eyring-Powell fluid over a stretching." *Results in Engineering* 14 (2022): 100435. https://doi.org/10.1016/j.rineng.2022.100435

[17] Arulmozhi, S., K. Sukkiramathi, Shyam Sundar Santra, R. Edwan, Unai Fernandez-Gamiz, and Samad Noeiaghdam. "Heat and mass transfer analysis of radiative and chemical reactive effects on MHD nanofluid over an infinite moving vertical plate." *Results in Engineering* 14 (2022): 100394. https://doi.org/10.1016/j.rineng.2022.100394

[18] Abu-Nada, Eiyad, and Ali J. Chamkha. "Effect of nanofluid variable properties on natural convection in enclosures filled with a CuO–EG–water nanofluid." *International Journal of Thermal Sciences* 49, no. 12 (2010): 2339-2352. https://doi.org/10.1016/j.ijthermalsci.2010.07.006

[19] Md Kasmani, Ruhaila, S. Sivasankaran, M. Bhuvaneswari, and Ahmed Kadhim Hussein. "Analytical and numerical study on convection of nanofluid past a moving wedge with Soret and Dufour effects." *International Journal of Numerical Methods for Heat & Fluid Flow* 27, no. 10 (2017): 2333-2354. https://doi.org/10.1108/HFF-07-2016-0277

[20] Wang, Fuzhang, Muhammad Awais, Rujda Parveen, M. Kamran Alam, Sadique Rehman, and Nehad Ali Shah. "Melting rheology of three-dimensional Maxwell nanofluid (graphene-engine-oil) flow with slip condition past a stretching surface through Darcy-Forchheimer medium." *Results in Physics* 51 (2023): 106647. https://doi.org/10.1016/j.rinp.2023.106647

[21] Wang, Fuzhang, Nainaru Tarakaramu, M. V. Govindaraju, Narsu Sivakumar, K. Bhagya Lakshmi, PV Satya Narayana, and Ramalingam Sivajothi. "Activation energy on three-dimensional Casson nanofluid motion via stretching sheet: Implementation of Buongiorno's model." *Journal of the Indian Chemical Society* 100, no. 2 (2023): 100886. https://doi.org/10.1016/j.jics.2023.100886

[22] Wang, Fuzhang, Muhammad Imran Asjad, Muhammad Zahid, Azhar Iqbal, Hijaz Ahmad, and M. D. Alsulami. "Unsteady thermal transport flow of Casson nanofluids with generalized Mittag–Leffler kernel of Prabhakar's type." *Journal of Materials Research and Technology* 14 (2021): 1292-1300. https://doi.org/10.1016/j.jmrt.2021.07.029

[23] Grosan, T., and I. Pop. "Axisymmetric mixed convection boundary layer flow past a vertical cylinder in a nanofluid." *International Journal of Heat and Mass Transfer* 54, no. 15-16 (2011): 3139-3145. https://doi.org/10.1016/j.ijheatmasstransfer.2011.04.018

[24] Yacob, Nor Azizah, Anuar Ishak, and Ioan Pop. "Falkner–Skan problem for a static or moving wedge in nanofluids." *International Journal of Thermal Sciences* 50, no. 2 (2011): 133-139. https://doi.org/10.1016/j.ijthermalsci.2010.10.008

[25] Bachok, Norfifah, Anuar Ishak, Roslinda Nazar, and Ioan Pop. "Flow and heat transfer at a general three-dimensional stagnation point in a nanofluid." *Physica B: Condensed Matter* 405, no. 24 (2010): 4914-4918. https://doi.org/10.1016/j.physb.2010.09.031

[26] Bachok, Norfifah, Anuar Ishak, and Ioan Pop. "Flow and heat transfer characteristics on a moving plate in a nanofluid." *International Journal of Heat and Mass Transfer* 55, no. 4 (2012): 642-648. https://doi.org/10.1016/j.ijheatmasstransfer.2011.10.047

[27] Hussain, Shahid, Kianat Rasheed, Aamir Ali, Narcisa Vrinceanu, Ahmed Alshehri, and Zahir Shah. "A sensitivity analysis of MHD nanofluid flow across an exponentially stretched surface with non-uniform heat flux by response surface methodology." *Scientific Reports* 12, no. 1 (2022): 18523. https://doi.org/10.1038/s41598-022-22970-y

[28] Shafiq, Anum, Tabassum Naz Sindhu, and Chaudry Masood Khalique. "Numerical investigation and sensitivity analysis on bioconvective tangent hyperbolic nanofluid flow towards stretching surface by response surface methodology." *Alexandria Engineering Journal* 59, no. 6 (2020): 4533-4548. https://doi.org/10.1016/j.aej.2020.08.007

[29] Wang, Xiang-Qi, and Arun S. Mujumdar. "A review on nanofluids-part II: experiments and applications." *Brazilian Journal of Chemical Engineering* 25 (2008): 631-648. https://doi.org/10.1590/S0104-66322008000400002

[30] Naseem, Faiza, Anum Shafiq, Lifeng Zhao, and Anum Naseem. "MHD biconvective flow of Powell Eyring nanofluid over stretched surface." *AIP Advances* 7, no. 6 (2017). https://doi.org/10.1063/1.4983014

[31] Reddy, Junuthula Narasimha. *An introduction to the finite element method*. New York: McGraw-Hill, 2019.

[32] Cortell, Rafael. "Viscous flow and heat transfer over a nonlinearly stretching sheet." *Applied Mathematics and Computation* 184, no. 2 (2007): 864-873. https://doi.org/10.1016/j.amc.2006.06.077